Solar Energy 207 (2020) 144–156

Contents lists available at ScienceDirect

Solar Energy

journal homepage: www.elsevier.com/locate/solener

Supercritical carbon dioxide cycles with multi-heating in Concentrating Solar Power plants

Luis F. González-Portillo*, Javier Muñoz-Antón, José M. Martínez-Val

Universidad Politécnica de Madrid, José Gutiérrez Abascal, 2, 28006 Madrid, Spain

ARTICLE INFO

Keywords:
Multi-heating
Solar tower
Supercritical
Concentrating Solar Power

ABSTRACT

This work analyses the features and performance of supercritical CO_2 cycles with multi-heating (heat supplies at different temperature) in Concentrating Solar Power plants, including its internal coherent integration. The specific features of multi-heating cycles fit perfectly with the characteristics of concentrating solar energy. The integration requires the design of a new type of solar field to accommodate the solar radiation hitting the receiver to the multi-heating requirements. This new solar field has a similar configuration to the solar tower, but receiver and heliostats are divided into two sections, and each section meets different requirements in concentration ratio, fluid temperature, and absorbed heat flux. This new solar field, called multi-heating solar tower, achieves higher efficiencies than standard solar towers with softer thermal requirements. The flexibility of the multi-heating structure is very useful to solve efficiently the restrictions of supercritical CO_2 cycles caused by the variations of specific heat close to the critical point. The resulting CSP plant with multi-heating achieves higher efficiency than plants with standard solar towers and supercritical CO_2 cycle.

1. Introduction

Concentrating Solar Power (CSP) plants with supercritical CO_2 (s-CO_2) cycles have been identified as the next generation of CSP systems (Mehos et al., 2017). S-CO_2 power cycles can achieve higher efficiency at potential lower costs than conventional power cycles. These improvements together with the intrinsic capacity of storing thermal energy from CSP makes the next generation of CSP systems a more competitive option for generating electricity, and several efforts are being carried out to find the optimum plant configuration.

The thermophysical properties of CO_2 allow s-CO_2 cycles to set the compressor inlet close to the critical point, which results in high cycle efficiency (González-Portillo et al., 2019; Rovira et al., 2014). Moreover, the CO_2 have other advantages such as its availability, low cost and very good thermal stability at high temperature (Dostal, 2004). For all these reasons, several researchers analyze the s-CO_2 as working fluid in CSP plants with different configurations (Binotti et al., 2017; Enríquez et al., 2017; Muñoz-Antón et al., 2015), and some of them even analyze the possibility of using this fluid as heat transfer fluid in the solar receiver (Muñoz-Anton et al., 2014).

National Renewable Energy Laboratory (NREL) and Sandia National Laboratories (SNL) suggest that the next generation of CSP plants should integrate s-CO_2 cycles and solar towers (Mehos et al., 2017). However, there are still several open questions, mainly the optimum type of receiver (Ho, 2017) and power cycle configuration (Crespi et al., 2017). Although these two topics must be deeply studied separately, the optimum CSP plant configuration will depend on the integration of its parts (González-Portillo et al., 2017). Several researchers have already analyzed different systems to try to elucidate the best option (Albrecht et al., 2019; Neises and Turchi, 2014; Padilla et al., 2016; Wang et al., 2017), but there are so many uncertainties that the best option is unclear yet.

Several different possibilities for the s-CO_2 cycle configuration have been proposed (Crespi et al., 2017). Two of the most promising ones are the simple and the recompression cycles (Dyreby, 2014). In the simple s-CO_2 cycle, five phases (compression, regeneration, heating, expansion and cooling) are enough to achieve high efficiencies at low cost. According to Ho et al (Ho et al., 2015), this configuration could be the optimum option to achieve the lowest cost of electricity in CSP systems. However, the large internal irreversibility in the regenerator (owing to the higher specific heat of the high-pressure side than that of the low-pressure side) lowers the efficiency of simple cycles, and other layouts are proposed to mitigate this problem. One of these layouts is the recompression cycle, which reduces the regeneration irreversibilities by means of an extra compressor in the middle of the regeneration. This cycle achieves higher efficiencies than the simple cycle, but at the

* Corresponding author.
E-mail address: lf.gonzalez@upm.es (L.F. González-Portillo).

https://doi.org/10.1016/j.solener.2020.06.066
Received 23 March 2020; Received in revised form 28 May 2020; Accepted 16 June 2020

Nomenclature

AHX	additional heat exchanger
A	area (m^2)
C	concentration ratio (-)
CSP	concentrated solar power
DNI	direct normal irradiance (W/m^2)
F	view factor (-)
h	specific enthalpy (kJ/kg)
$\dot{H}$	enthalpy (W)
htc	heat transfer coefficient (W/m^2K)
HTF	heat transfer fluid
HTR	high-temperature regenerator
LTR	low-temperature regenerator
MHC	multi-heating cycle
MHST	multi-heating solar tower
P	Pressure (kPa)
PHX	primary heat exchanger
q	heat (kJ/kg)
$\dot{Q}$	thermal power (W)
SC	simple cycle
ST	solar tower
S-CO₂	supercritical carbon dioxide
T	Temperature (°C)
U	heat transfer coefficient from receiver surface to fluid (W/m^2 K)
w	specific work (J/kg)
$\dot{W}$	power (W)

Greek symbols

A	absorptivity (-)
E	effectiveness (-)
ε_r	Emissivity (-)
H	Efficiency (-)
Σ	Stefan–Boltzmann constant (W/m^2 K^4)

Subscripts

ah	additional heat
c	compressor
crit	critical
cv	convection
cycle	cycle
geo	geometrical
hel	heliostats
HTF	heat transfer fluid
in	inlet
opt	optical
ph	primary heat
rad	radiation
rec	receiver
syst	system
t	turbine

expense of a more complex system with an extra compressor. Different parameters (such as operating conditions or components cost) will determine if the simplicity of simple cycles outweighs or not the higher efficiency of recompression cycles (Bryant et al., 2011).

Another possibility to reduce the internal irreversibility in the regenerator is the use of heat sources at low temperature (Ahn et al., 2014; González-Portillo et al., 2020; Kim et al., 2012; Linares et al., 2015; Syblik et al., 2019). Although the layout may differ from a source to the other, the concept is the same: additional heat sources at low temperature supply part of the thermal power reducing the power supplied at high temperature, which involves an increase in the exergy efficiency (González-Portillo et al., 2020). The problem of providing additional energy sources at different temperatures must be solved according to the origins of the available heat in the power plant. This is difficult to do with combustion devices, where the combustion products should be generated with the maximum achievable temperature. However, there are some alternatives presented in the literature. Kim et al (Kim et al., 2012) proposes the application of cycles with heat supplies at high- and low-temperature in nuclear power plants. The cycle would operate only with the high-temperature heat source (nuclear energy) when the demand of electricity is low, and the waste heat would be stored in a low-temperature thermal energy storage. When the demand of electricity is high, the cycle with the low-temperature heat source (the storage) and the high-temperature heat source (nuclear energy) can produce more power thanks to an efficiency 10% greater. Linares et al (Linares et al., 2015) analyze the thermal efficiency of s-CO_2 cycles with low-temperature heat sources for fusion reactors. The result is that electric power and efficiency are improved more than 5% by “matching in a proper way all the available thermal sources” (Linares et al., 2015). More researchers have kept studying these cycles for fusion energy due to the promising results (Syblik et al., 2019). Other studies analyze cycles with heat supplies at low- and high-temperature, but using the same heat source (Ahn et al., 2014). The result is a lower efficiency than in simple cycles since the objective of these cycles is to better fit with the temperature range imposed by the thermal source.

The use of heat sources at low temperature to increase the system efficiency has been analyzed in nuclear and fusion energy, but not in CSP, where the heat can be adjusted within a selected range of temperatures, according to solar conditions, concentrator field and receiver features (Muñoz et al., 2009). Thus, the purpose of this paper is to integrate s-CO_2 cycles with heat supplies at high- and low-temperature into CSP plants and analyze the system efficiency. This integration will require the design of a new type of solar field to accommodate the features of solar energy to the multi-heating (at different temperatures) requirements. Moreover, while most of the cycles including low-temperature sources supply the heat from the compressor outlet temperature to the primary heat inlet temperature (Ahn et al., 2014; Linares et al., 2015; Syblik et al., 2019), the cycle used in this study can change these temperatures following the layout proposed by Kim et al (Kim et al., 2012). Thus, while the former cycles are generally called preheating cycles (Crespi et al., 2017), the cycles used in this paper will be called multi-heating cycles. The CSP plant presented in this study, and so the analysis, has not been previously analyzed to the best of the authors knowledge.

The main optimization objective in the new CSP multi-heating system is to reduce entropy generation in the heating process by fitting the temperature level of the thermal feeding of a given component to the role of such component in the cycle. The reduction of entropy generation in multi-heating cycles has been previously addressed in previous research (González-Portillo et al., 2020), so this study focuses on the application to CSP systems. Different design conditions of the cycle involve different thermal requirements for the heat source. This study analyzes different operating conditions in the system (in cycle and solar field) to look for the maximum efficiency.

Section 2 describes the new system and the model used to calculate its efficiency. This model is separated into two parts: s-CO_2 cycle and solar field (which includes receiver and concentrator). The efficiency of the new CSP system will be compared with the results of a CSP plant composed of a solar tower and a simple s-CO_2 cycle. Similarities between the two systems are described in Section 2, and the efficiencies are compared in Section 3. The influence of the main variables in the

solar field (concentration ratio and temperatures) and cycle (pressures and temperatures) in the cycle is analyzed in this section. Numerical results show the advantages of dividing a receiver into sections to meet different requirements in radiation concentration and fluid temperature. Conclusions and future work will close the paper in Section 4.

2. CSP plant model

Two types of CSP plant are compared in this study: a standard Solar Tower integrated with a simple regenerative s-CO_2 cycle and a Multi-Heating Solar Tower integrated with a multi-heating s-CO_2 cycle. Figs. 1 and 2 show the configuration of these plants. In the standard system, there is a single heat supplied by a set of heliostats through a single receiver and the primary heat exchanger (PHX). On the other hand, in the multi-heating system there are two heat supplies, and each heat has its own set of heliostats, receiver section and heat exchanger. In this way, the primary heat is supplied by the PHX, and the additional heat by the additional heat exchanger (AHX). This AHX is located in the middle of the regeneration. Thus, while there is a single regenerator in the standard system, there are two in the multi-heating system: a low-temperature regenerator (LTR) and a high-temperature regenerator (HTR). The rest of components (precooler, compressor and turbine) are the same in both systems.

The heat supply in the standard system works at a specific range of temperatures and concentration ratios. On the other hand, the multi-heating plant shown in Fig. 2 can supply the heat at two different ranges of temperature and concentration ratio. A greater number of heat supplies at different ranges of temperature could achieve higher efficiencies. However, our previous research showed that the benefit of adding a third heat supply is small and it probably does not outweigh the extra complexity that adheres (González-Portillo et al., 2020).

The software Engineering Equation Solver (Klein, 1992) is used to model the standard and the multi-heating CSP systems. Both systems are divided into two subsystems that can be analyzed separately: power cycle and solar field. The efficiency of these two subsystems will define the system efficiency as:

$$\eta_{syst} = \eta_{SF}\eta_{cycle} \tag{1}$$

where η_{SF} is the solar field efficiency (which integrates receiver and heliostats) and η_{cycle} the cycle efficiency. The following sections describe the models of the cycles and the receivers, its validation and the calculation of its efficiencies.

2.1. Supercritical CO_2 cycle

Fig. 3 represents the layout of a simple s-CO_2 cycle and a multi-heating s-CO_2 cycle in the same P-h and T-s diagrams. The four main parts of both thermodynamic cycles, compression ($w_c = h_2 - h_1$), heating ($q_{heat} = h_4 - h_2$), expansion ($w_t = h_4 - h_5$) and cooling ($q_{cool} = h_5 - h_1$), are the same. The difference is the management of the heat sources, which are represented in blue for the simple cycle and in red for the multi-heating cycle. While the simple cycle has just one heat supply at high temperature in the primary heat exchanger ($q_{PHX} = h_4 - h_3$), two heats are supplied to the multi-heating cycle, one of them at high temperature in the primary heat exchanger ($q_{PHX} = h_4 - h_{3'}$), and the other at a low temperature in the additional heat exchanger ($q_{AHX} = h_{8'} - h_{7'}$). In this way, while the simple cycle has one regenerator, the multi-heating cycle has two: LTR and HTR. Note that the maximum additional-heat temperature ($T_{8'}$) is limited to the minimum primary-heat temperature ($T_{3'}$).

Kim et al (Kim et al., 2012) analyze a cycle similar to the multi-heating cycle presented in Figs. 2 and 3. The only difference is that, while the cycle from this study supplies the additional heat after the LTR, the cycle from Kim et al supplies the additional heat to/during the LTR. While the layout is different, the cycle analysis is the same since the limiting factor is point 8′, which is the maximum additional-heat temperature in Fig. 3 and the maximum LTR temperature in the cycle from Kim et al. This means that both cycle will have the same efficiency if point 8′ is the same.

Special attention must be paid to the definition of the regenerator size in order to make a fair comparison between simple and multi-heating cycles. Since there are no differences in the low-pressure side of both cycles, an effectiveness for the regeneration of this side is defined as follows:

$$\varepsilon = \frac{h_5 - h_6}{h_5 - h_{T2,P6}} \tag{2}$$

where $h_{T2,P6}$ is the enthalpy of the point defined by pressure of point 6, P6, and temperature of point 2, T2. This definition was introduced by Padilla et al (Padilla et al., 2015) to compare other type of cycles with two regenerators. In this way, a simple and a multi-heating cycle with the same points 1245 and the same global effectiveness will have the same point 6.

In the case of the multi-heating cycle, another effectiveness is needed to define the whole regeneration process. Following previous definition of effectiveness, the HTR effectiveness will be defined as:

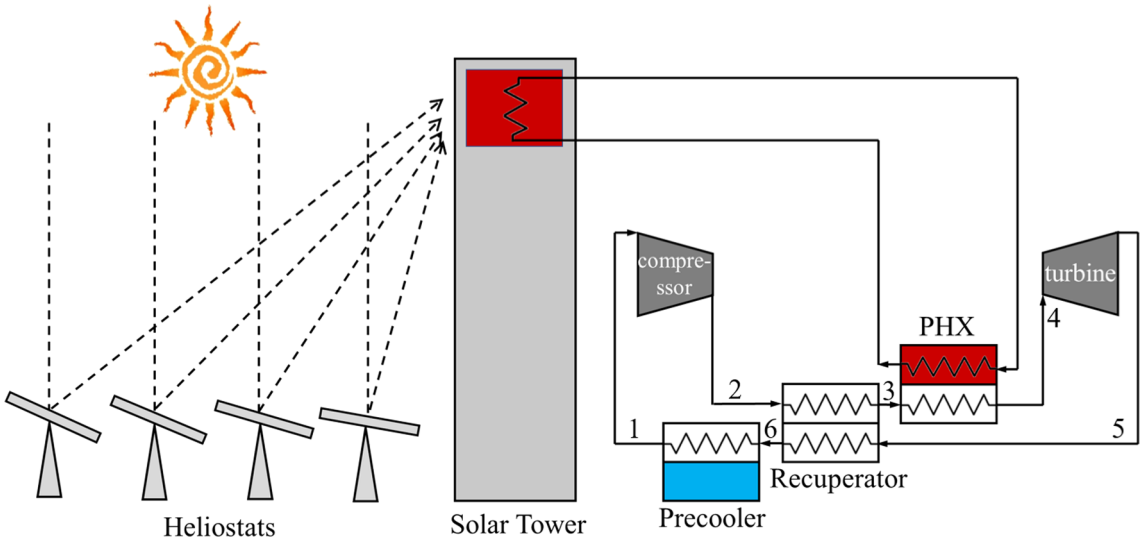

Fig. 1. CSP plant with standard Solar Tower and simple regenerative s-CO_2 cycle.

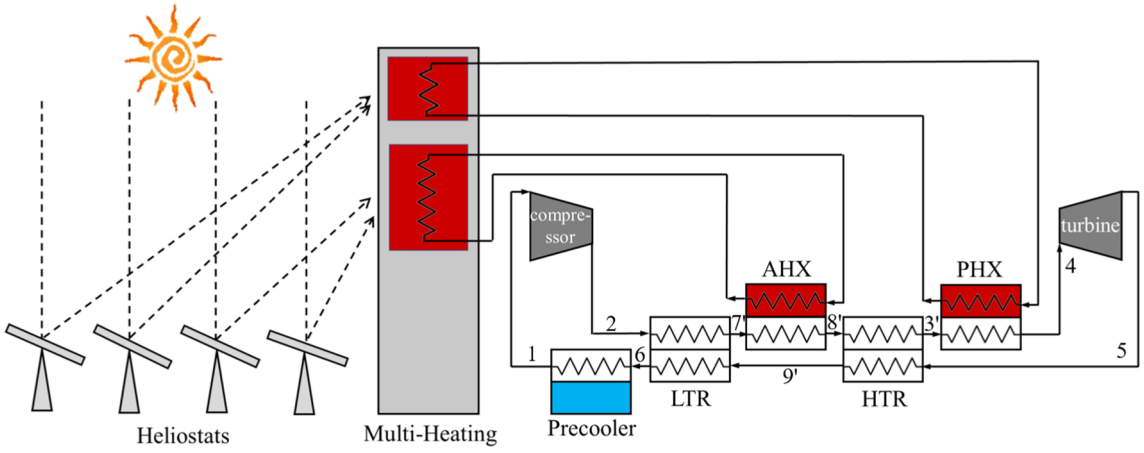

Fig. 2. CSP plant with Multi-Heating Solar Tower and multi-heating s-CO_2 cycle.

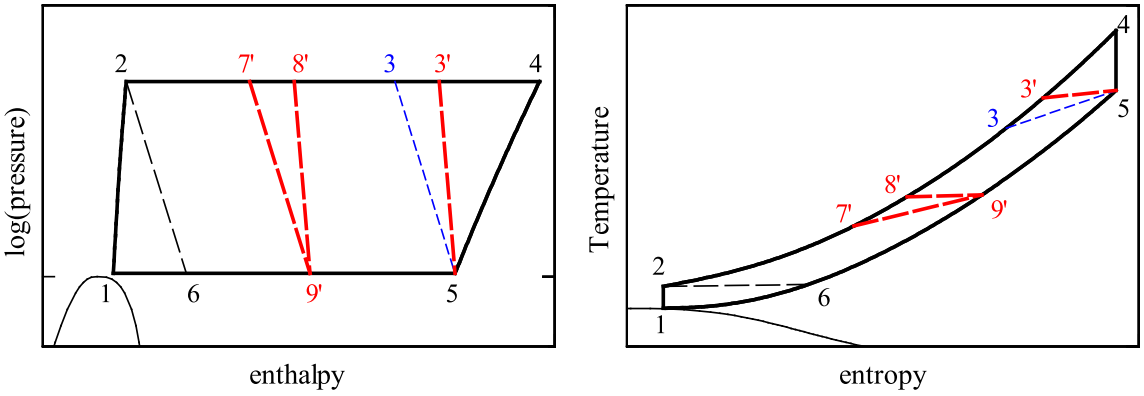

Fig. 3. Layout of a simple s-CO_2 cycle (black and blue) and a multi-heating s-CO_2 cycle (black and red) in diagrams pressure-enthalpy and temperature-entropy.

$$\varepsilon_{HTR} = \frac{h_5 - h_{9'}}{h_5 - h_{T8',P9'}} \tag{3}$$

The effectiveness of the LTR will be an output when the effectiveness defined in Eqs. (2) and (3) and the additional-heat maximum temperature are defined.

Table 1 lists the cycle design parameters and variables used for the analysis of simple and multi-heating s-CO_2 cycles in the reference case. These parameters are consistent with the literature (Neises and Turchi, 2019; Padilla et al., 2015). The maximum additional-heat temperature will be a variable in all the simulations. Moreover, high- and low-side pressures and compressor and turbine inlet temperatures shown in Table 1 are used as reference case, but they will also be variables. Pressure drops are neglected.

The values from Table 1 will be used to calculate the cycle efficiency, defined as:

$$\eta_{cycle} = \frac{\dot{W}_t - \dot{W}_c}{\dot{Q}_{total}} \tag{4}$$

where $\dot{Q}_{total}$ is the sum of all the thermal powers supplied to the cycle. The resulting cycle efficiency is validated with the results from (Padilla et al., 2015) for the case of the simple cycle. The same results are obtained for turbine inlet temperatures from 500 °C to 850 °C (range of temperatures analyzed in (Padilla et al., 2015)).

The cycle efficiency can also be expressed as:

$$\eta_{cycle} = \frac{1 - \frac{\dot{W}_c}{\dot{W}_t}}{\frac{\dot{Q}_{total}}{\dot{W}_t}} = \frac{1 - \frac{\dot{W}_c}{\dot{W}_t}}{1 + \frac{\Delta\dot{H}_{loss}}{\dot{W}_t}} \tag{5}$$

where

$$\Delta\dot{H}_{loss} = \dot{H}_5 - \dot{H}_3 = \dot{H}_{9'} - \dot{H}_{7'} \tag{6}$$

Eq. (5) helps to realize that cycle efficiency is the same in simple and multi-heating cycles defined by the same parameters. The difference between these two type of cycles is the region of the thermodynamic diagram where the term called $\Delta\dot{H}_{loss}$ is placed in Fig. 3: between points 3 and 5 in the case of simple cycle and between points 7′ and 9′ in the case of multi-heating cycle. This means that the difference between the simple and the multi-heating cycle is the temperature of the supplied heat $\Delta\dot{H}_{loss}$. If the heat source efficiency is higher at low temperature then the efficiency of a system integrating multi-heating will be higher thanks to the additional heat at low temperature.

The term $\Delta\dot{H}_{loss}$ appears in s-CO2 cycles due to the strong variation of thermodynamic properties close to the critical point (T_{crit} = 31 °C, P_{crit} = 7.4 MPa), and involves high internal irreversibilities in the regenerator. Fig. 4 shows the specific heat variation as a function of temperature at the high- and low-side pressures defined in Table 1. The

Table 1
Parameters used to analyze simple and multi-heating s-CO_2 cycles.

Parameter	Value
Maximum high-side pressure, P_H	25 MPa
Minimum low-side pressure, P_L	9 MPa
Compressor inlet temperature, $T_{c,in}$	40 °C
Maximum additional-heat temperature, T_{ah}	variable
Turbine inlet temperature, $T_{t,in}$	700 °C
Compressor efficiency, η_c	0.89
Turbine efficiency, η_t	0.9
Global effectiveness, ε	0.95
HTR effectiveness, ε_{HTR}	0.95
Net power	50 MW_e

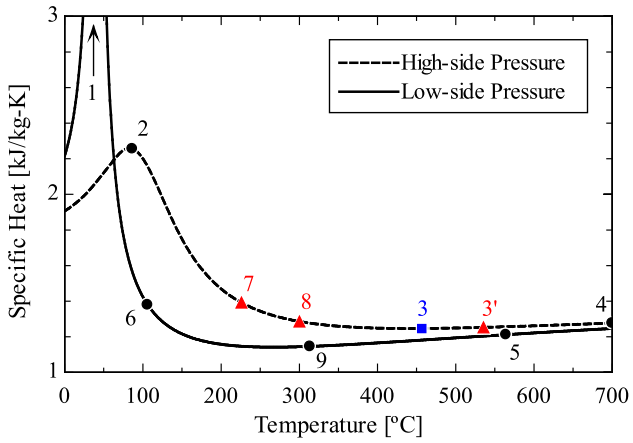

Fig. 4. Specific heat as a function of temperature at high- and low-side pressure of a s-CO_2 cycle. The points are from a simple s-CO_2 cycle (black and blue) and a multi-heating s-CO_2 cycle (black and red).

cycle points from the cycles in Fig. 3 are also represented. The big difference in specific heat at one end of the heat exchanger (points 2 and 6) is translated to an increase of temperature at the other end of the heat exchanger (points 3 and 5 in the simple cycle and points 7 and 9 in the multi-heating cycle), where the specific heat is similar in both pressure sides. In this way, a heat is needed to compensate this temperature difference. The value of this heat is the same in the simple and the multi-heating cycle (very close to $\Delta\dot{H}_{loss}$), but it is supplied at different temperature.

The term $\Delta\dot{H}_{loss}$, necessary for the use of multi-heating, increases when the compressor inlet temperature is close to the critical temperature. For example, Fig. 4 shows the case of compressor inlet temperature $T_{c,in}$ = 40 °C. If this temperature were smaller, e.g., $T_{c,in}$ = 32 °C, then the difference in specific heat would be greater between points 2 and 6, resulting in a greater value of $\Delta\dot{H}_{loss}$ and so a bigger additional heat. The lower the compressor inlet temperature, the greater the potential of multi-heating is.

2.2. Solar field

The solar field is the part in charge of supplying thermal power to the power cycle. It integrates heliostat field, in charge of concentrating the solar radiation, and receiver, in charge of absorbing this radiation. In the case of a multi-heating system, the solar field is divided into two sections. Each section supplies the thermal power within a specific range of temperatures and a specific flux of solar radiation. The value of these parameters (temperature and solar heat flux) will determine the amount of thermal power that the HTF absorbs, $\dot{Q}$, in relation to the total power reaching the heliostat field, $\dot{Q}_{SF}$, which is the definition of solar field efficiency, η_{SF}:

$$\eta_{SF} = \frac{\dot{Q}}{\dot{Q}_{SF}} \tag{7}$$

Since the multi-heating system is divided into sections, the solar field efficiency can also be expressed as:

$$\eta_{SF} = \frac{\sum \dot{Q}_i}{\sum \dot{Q}_{SF,i}} = \frac{\sum \dot{Q}_i}{\sum \frac{\dot{Q}_i}{\eta_{opt,i}\eta_{rec,i}}} \tag{8}$$

where i represents the section of the multi-heating system (primary and additional), η_{opt} the optical efficiency of the heliostat field, and η_{rec} the receiver efficiency.

The thermal power that the HTF must absorb is imposed by the power cycle. Optical and receiver efficiencies are calculated with the models described in the following sections.

2.2.1. Receiver

The thermal power reaching the receiver is defined in Eq. (9), where A_{hel} is the area of the heliostats field, *DNI* the Direct Normal Irradiance and η_{opt} the optical efficiency of the concentration process.

$$\dot{Q}_{rec} = A_{hel}\eta_{opt}DNI \tag{9}$$

All this power is concentrated in the receiver area. The concentration is defined by a dimensionless parameter called geometrical concentration ratio, that relates heliostats and receiver area:

$$C_{geo} = \frac{A_{hel}}{A_{rec}} \tag{10}$$

If the concentration ratio considers the optical efficiency, then it is called optical concentration ratio:

$$C_{opt} = \eta_{opt}C_{geo} \tag{11}$$

And Eq. (9) can be redefined as:

$$\dot{Q}_{rec} = A_{rec}C_{opt}DNI \tag{12}$$

Part of the radiation reaching the receiver is absorbed by the HTF and the rest is lost. The receiver efficiency is defined as the power absorbed by the HTF, $\dot{Q}_{HTF}$, divided by the power reaching the receiver, $\dot{Q}_{rec}$:

$$\eta_{rec} = \frac{\dot{Q}_{HTF}}{\dot{Q}_{rec}} \tag{13}$$

Eq. (14) represents the energy balance to the receiver.

$$\alpha\cdot\dot{Q}_{rec} = \dot{Q}_{HTF} + \dot{Q}_{cv} + \dot{Q}_{rad} \tag{14}$$

The left term represents the thermal power absorbed by the receiver, where α is the receiver absorptivity, and the right term is the sum of the thermal power transmitted to the HTF, $\dot{Q}_{HTF}$, and the convection and radiation losses, $\dot{Q}_{cv}$ and $\dot{Q}_{rad}$, respectively. The thermal powers belonging to the right term are defined in Eqs. (15)–(17).

$$\dot{Q}_{HTF} = A_{rec}\cdot U\cdot(T_{rec} - T_{HTF}) \tag{15}$$

$$\dot{Q}_{cv} = A_{rec}\cdot htc\cdot(T_{rec} - T_{air}) \tag{16}$$

$$\dot{Q}_{rad} = A_{rec}\cdot F\cdot\varepsilon_r\cdot\sigma\cdot({T_{rec}}^4 - {T_{sky}}^4) \tag{17}$$

The receiver surface is considered to be at the same temperature, T_{rec}, in internal and external surfaces, i.e., in the surface in contact with the HTF and in the surface in contact with the environment. The heat transfer coefficient from receiver surface to HTF, U, determines the capacity of the receiver to transfer heat to the HTF with a temperature T_{HTF}. Moreover, the receiver also exchanges heat with the environment, by convection with the air and by radiation with the sky. The heat transfer coefficient from receiver surface to air, *htc*, defines convection losses and view factor, F, and receiver emissivity, ε_r, define radiation losses. Note that the radiation losses are simplified considering that the heat exchange is only against the sky, where the sky temperature, T_{sky}, is calculated as a function of the air temperature (Swinbank, 1963):

$$T_{sky} = 0.0552\cdot{T_{air}}^{1.5}(K) \tag{18}$$

The thermal power that the HTF absorbs is imposed by the thermal power that the cycle needs. A heat exchanger supplies the thermal power from the solar field to the cycle. The model assumes a temperature difference ΔT = 25 °C (Ho et al., 2016) between the s-CO_2 and the HTF both in the primary heat exchanger as in the additional heat exchanger.

Table 2 shows the input parameters used in the analysis of the solar field. DNI is a representative value of summer in Dagget (USA) (EnergyPlus, 2018). The rest of the values are common values used in CSP simulations (Ho and Iverson, 2014; Muñoz et al., 2011; Padilla et al., 2015). The value of the heat transfer coefficient from receiver surface to HTF, U, will depend on the fluid features and the receiver

Table 2
Parameters used to analyze the solar field.

Parameter	Value
Optical efficiency	0.6
Geometrical concentration ratio	1000
Direct Normal Irradiance	950 W/m^2
Emissivity primary heat section	0.85
Emissivity additional heat section	0.15
Absorptivity	0.95
View factor	1
Heat transfer coefficient from receiver surface to air	5 W/m^{2}K
Heat transfer coefficient from receiver surface to fluid	10 kW/m^{2}K

design. This study sets a typical value from molten salts (Wang et al., 2020). The maximum possible view factor, F, is set in order to consider the worst-case scenario. The value of this factor will also depend on the receiver design.

Emissivity and absorptivity properties from Table 2 are given by the receiver coating. The coating commonly used in solar towers is Pyromark®. This coating has a high solar absorptance ($\alpha \sim 0.95$), but also high emittance (0.85) (Ho and Iverson, 2014; Padilla et al., 2015). Other coatings such as cermet coatings (currently used in linear receivers) have better optical properties ($\varepsilon_r \sim 0.15$ (Forristall, 2003; Montes et al., 2009; Muñoz et al., 2011)). However, they are sensitive to oxidation and suffer performance degradation at temperatures greater than 500 ˚C, and therefore they are not well-suited for solar tower applications, where higher temperatures are reached. The multi-heating receiver will use Pyromark® in the primary heat section and cermet coating in the additional-heat section, which works at low temperature.

The receiver model presented in this study is composed of simple equations, which represent the main characteristics of the system and allows to focus on the main physics of the problem. The trends in the results obtained with more complex model should be similar, and the differences would be mainly due to the receiver design. Fig. 5 shows that, effectively, the simplistic model presented in this study obtains similar results to those obtained with more complex and mature models such as the software System Advisor Model (SAM) (NREL, 2018). More information about the results obtained with SAM can be found in the Appendix.

Both the EES model and SAM show the same trend: the receiver efficiency decreases with the temperature. Thus, the additional heat supplied at low temperature in the multi-heating system will increase the system efficiency. Moreover, the receiver efficiency increases with the solar heat flux up to an asymptote, which depends on the temperature. Beyond this asymptote, the receiver efficiency does not increase, but the required concentrator gets more complex and less efficient. The optical efficiency in the heliostat field will determine the optimal concentration for each temperature.

2.2.2. Heliostat field

The optical efficiency of the heliostat field is defined as the ratio between the radiation hitting the receiver, $\dot{Q}_{rec}$, and the solar radiation reaching the heliostat field, $\dot{Q}_{sun}$:

$$\eta_{opt} = \frac{\dot{Q}_{rec}}{\dot{Q}_{sun}} \tag{19}$$

The optical efficiency will be determined by the heliostat field configuration. The software SolarPILOT (Wagner and Wendelin, 2018) is used to simulate different CSP plants with solar tower. The area of heliostats and its optical efficiency are calculated for different receiver areas. The main parameters used for these simulations are shown in Table 3. The concentration ratio is calculated from the ratio of heliostats and receiver areas and so every concentration ratio will have associated an optical efficiency.

Fig. 6 shows the optical concentration as a function of the optical concentration ratio obtained with SolarPILOT. The optical efficiency $\eta_{opt} = 0.6$ at optical concentration ratio $C_{opt} = 600$ agrees with the value used in other studies about solar towers (Ho and Iverson, 2014; Padilla et al., 2015). This value is used for the standard Solar Tower and for the primary-heat section of the Multi-Heating Solar Tower. The optical concentration ratio in the additional-heat section will be modified to maximize the efficiency of the solar field (receiver + heliostat field). Since there is a big range of solar heat flux to achieve high receiver efficiencies when the temperature is low (see Fig. 5), low concentration ratios will be preferred to increase the optical efficiency, and so the solar field (receiver + heliostats) efficiency.

Results from SolarPILOT in Fig. 6 are obtained for the values from Table 3. In a proper design of a multi-heating solar tower, the solar field would have to be divided into two parts and designed separately with different parameters. The low concentration ratios in the additional-heat section could lead to different designs in the solar tower. For example, the thermal power to the additional-heat section could be supplied by the spillage of the primary-heat section, or even by Parabolic Trough collectors with low concentration ratios ($C_{opt} \sim 50$) but high optical efficiencies ($\eta_{opt} \sim 0.7$). Anyway, Fig. 6 helps to make a first approximation of the optical efficiency when optical concentration in the additional-heat section is reduced.

3. Results

This section shows the benefits of a multi-heating CSP system (multi-heating solar tower and multi-heating s-CO_2 cycle) by comparing it to a standard CSP system (standard solar tower and simple s-CO_2 cycle). In order to do so, the benefits of a specific multi-heating solar tower are shown first. Then, the multi-heating solar tower will be optimized for different power cycle conditions and the performance of the whole plant will be analyzed.

3.1. Additional-heat temperature

The thermal power in a multi-heating cycle is supplied by the primary heat section and the additional heat section. The amount of thermal power for each section depends on the additional-heat temperature. Fig. 7 shows the thermal power distribution in a multi-heating cycle with the conditions from Table 1 as a function of the maximum temperature in the additional heat ($T_{8'}$ in Fig. 3). The total thermal power is the sum of the thermal power in its two sections: primary heat and additional heat. Since the total power is constant, the additional heat substitutes the primary heat when the additional-heat temperature increases. Note that the case with null additional heat would

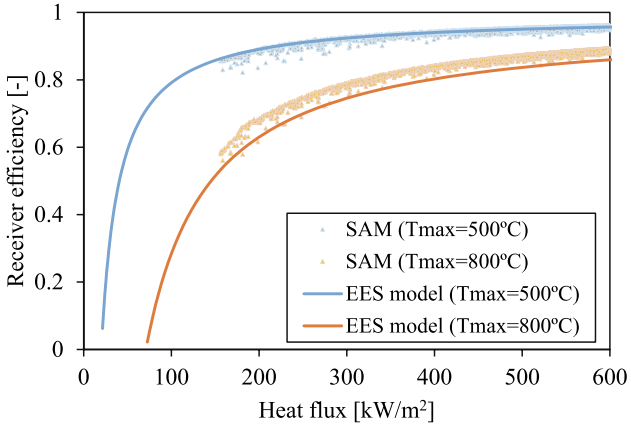

Fig. 5. Receiver efficiency as a function of heat flux for different maximum HTF temperatures (Tmax). Results from the EES model presented in this study are compared to results from System Advisor Model (SAM).

Table 3
Main parameters of heliostat field.

Parameter	Value
Location	Dagget
Month/day/hour	3/20/12
Tower height	200 m
Design power	750 MWt
Receiver aspect ratio	1
Receiver horizontal acceptance angle	360°
Total reflected image error	4 mrad

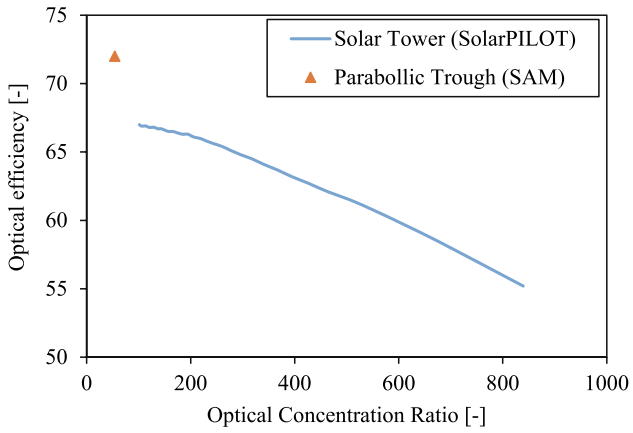

Fig. 6. Optical efficiency of a heliostat field and a Parabolic Trough as a function of optical concentration ratio.

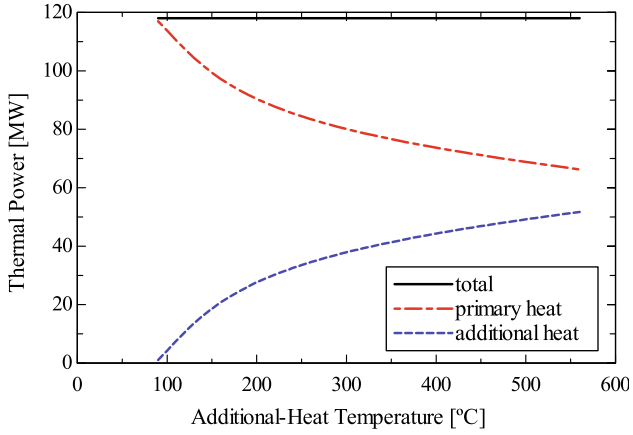

Fig. 7. Thermal power distribution in a multi-heating cycle and a Multi-Heating Solar Tower as a function of additional-heat temperature in the cycle.

correspond to a simple cycle, and the case with maximum additional heat to a multi-heating cycle where additional and primary heats are supplied one behind the other (maximum additional-heat temperature, $T_{8'}$, is the minimum primary-heat temperature, $T_{3'}$).

The thermal power shown in Fig. 7 will be supplied by a Multi-Heating Solar Tower (MHST). If the additional-heat temperature in the cycle is T_{ah}, the corresponding HTF temperature will be T_{ah} + 25 °C. Thermal power and temperature allow to calculate the receiver efficiency. Fig. 8 shows the receiver efficiencies of a MHST with the conditions from Table 2 coupled to the multi-heating cycle from Fig. 7. The receiver efficiencies are represented as a function of the maximum additional-heat temperature in the cycle.

The efficiency of the primary heat is constant since the maximum temperature of this heat does not change. On the other hand, the additional-heat efficiency decreases with the additional heat temperature. Nonetheless, this efficiency is higher than the efficiency in the primary heat, which involves an increase in the total receiver efficiency. While the receiver efficiency in the additional heat decreases with the temperature, its thermal power supply increases. The result is an optimum additional-heat temperature for which the maximum efficiency of the Multi-Heating Solar Tower is achieved. In Fig. 8, this temperature is T_{ah} = 560 °C and the efficiency η_{rec} = 87.5%. The additional thermal power in this optimal configuration represents 44% of the total power supplied by the Multi-Heating Solar Tower. Despite the maximum efficiency is obtained at a temperature T_{ah} = 560 °C, lower temperatures also get high receiver efficiencies. For example, if the temperature is T_{ah} = 300 °C the efficiency is η_{rec} = 86.8% and the additional thermal power represents a 32% of the total power. The advantage of lower temperatures is to obtain softer thermal requirements and so potential lower costs.

Note that the case with no additional heat represents a simple regenerative cycle coupled to a standard Solar Tower (ST). The receiver efficiency of this receiver is 83.7%. Thus, according to the results from Fig. 8, the maximum receiver efficiency of the MHST (achieved at T_{ah} = 560 °C) is 3.8% greater than the receiver efficiency of a standard ST. In the case of a temperature T_{ah} = 300 °C the receiver efficiency of the MHST would still be 3.1% greater.

3.2. Concentration ratio

The receivers simulated in Fig. 8 are designed to receive a solar radiation with optical concentration ratio C_{opt} = 600, which is characteristic of Solar Towers. In order to compare the MHST with a standard ST, the optical concentration ratio of the primary heat of the MHST and the standard ST will be set to C_{opt} = 600. However, this value seems too high for the low temperatures of the additional-heat section. Thus, the influence of the optical concentration ratio in the additional heat is analyzed.

Fig. 9 shows the effect of varying the concentration ratio in the additional-heat section of two MHST: one with additional-heat temperature T_{ah} = 300 °C and the other with T_{ah} = 560 °C. The receiver efficiencies of these two MHST are represented as a function of the concentration ratio in the additional-heat section. Moreover, the efficiency of the two sections (primary and additional heat) in the MHST with additional-heat temperature T_{ah} = 300 °C are also shown to understand the behavior of the whole MHST.

The receiver efficiency of the primary-heat section remains constant since its optical concentration ratio has been set to $C_{opt,ph}$ = 600. The MHST efficiency has a value in between the efficiency of its two sections, following the tendency of the additional-heat efficiency: it rapidly increases at low concentrations and then asymptotes. The receiver efficiency increases slowly from this value onwards.

When the concentration ratio is $C_{opt,ah}$ = 600, the efficiency of the

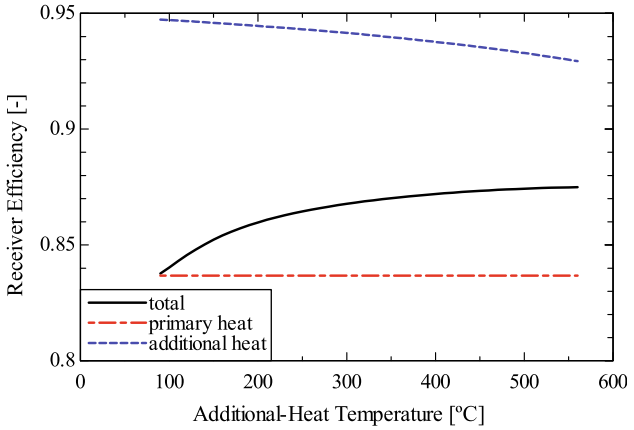

Fig. 8. Receiver efficiencies in a Multi-Heating Solar Tower as a function of additional-heat temperature in the cycle.

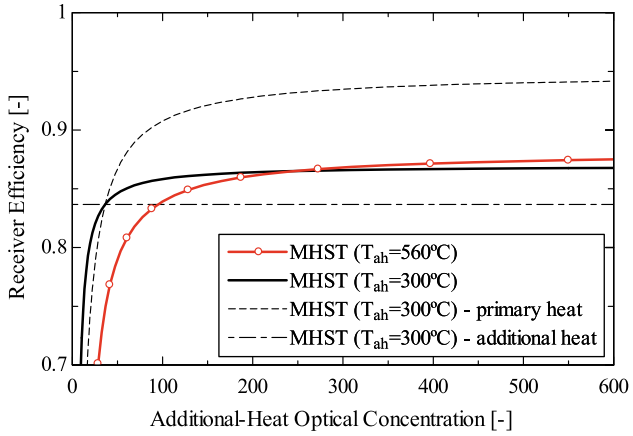

Fig. 9. Receiver efficiency of Multi-Heating Solar Towers (MHST) with additional-heat temperatures T_{ah} = 300 °C and T_{ah} = 560 °C as a function of concentration ratio for the additional-heat section.

MHST with additional-heat temperature T_{ah} = 560 °C is greater than when the additional-heat temperature is T_{ah} = 300 °C. This is the result also shown in Fig. 8. However, at low concentration ratios, e.g., at $C_{opt,ah}$ = 100, the MHST with additional-heat temperature is T_{ah} = 300 °C achieves a greater efficiency. The optimum additional-heat temperature will depend on the concentration ratio.

Note that the efficiency of a Solar Tower is the same than the efficiency of the primary heat in the MHST since the maximum temperature is the same in both cases. Thus, the efficiency of the MHST with additional-heat temperature T_{ah} = 300 °C is higher than the efficiency of the Solar Tower when the concentration ratio is greater than $C_{opt,ah}$ = 37. In the case of additional-heat temperature T_{ah} = 560 °C, this concentration ratio is $C_{opt,ah}$ = 95. If the concentration ratio were, for example, $C_{opt,ah}$ = 100, the efficiency of the MHST with additional-heat temperature T_{ah} = 560 °C would be almost the same than the efficiency of the ST, but the efficiency of the MHST with additional-heat temperature T_{ah} = 300 °C would be 2.1% greater than the Solar Tower efficiency. A smaller heat flux involves a lower temperature difference between inner and outer surface of the receiver, which involve smaller thermal stresses (Neises et al., 2014). Therefore, the MHST would not only have the advantage of greater efficiency, but also would involve softer thermal requirements, which has the potential to reduce the complexity of the receiver and, therefore, the cost.

Beside softer thermal requirements, smaller concentrations have another advantage: higher optical efficiencies (see Fig. 6). The efficiency of the solar field (which integrates receiver and concentrator) is calculated for three systems: standard Solar Tower, Multi-Heating Solar Tower with the additional-heat temperature T_{ah} = 300 °C, and Multi-Heating Solar Tower with the additional heat temperature optimized to maximize the efficiency. The additional-heat temperature is set to T_{ah} = 300 °C in one of the cases to have it as reference as greater efficiencies can be achieved at the expense of higher temperatures. Fig. 10 represents the efficiency of the mentioned solar fields as a function of the additional-heat concentration ratio.

The efficiency is constant in the case of the ST since the additional-heat concentration ratio does not vary. In the cases with MHST, the efficiency increases at low concentration ratios following the trend of the receiver efficiency in Fig. 9, and decreases at high concentration ratios following the trend of the optical efficiency in Fig. 6. The result is a maximum MHST efficiency at concentration ratio $C_{opt,ah}$ = 135 in the case of additional heat temperature T_{ah} = 300 °C and at concentration ratio $C_{opt,ah}$ = 200 in the case of optimized additional heat temperature. At these points, the difference between the efficiency of MHST and ST are 3.2% and 3.6%, respectively.

The additional-heat temperature determines the portion of additional power supplied to the cycle. Fig. 11 shows the additional-heat temperature and the portion of additional power as a function of the concentration ratio. In the case of the MHST with additional heat temperature T_{ah} = 300 °C, the additional power represents a 32.1% of the total power. However, this portion varies with the concentration ratio in the MHST with the optimized additional heat temperature since this temperature changes. Greater concentrations allow to achieve higher temperatures with high efficiency, and higher additional-heat temperatures mean bigger thermal powers, as shown in Fig. 7. The amount of additional thermal power is constant for concentration ratios above C_{ah} = 300 since the additional-heat temperature gets to a maximum, which is the minimum primary-heat temperature.

The solar field of MHST has shown to achieve higher efficiencies than ST with softer thermal requirements. Although the results shown analyze the solar field, the cycle is implicitly taken into account since it determines the thermal power needed and its range of temperatures. The cycle used till now is defined by the design parameters in Table 1. The efficiency of this cycle is η_{cycle} = 42.4% either in the case of simple or multi-heating cycle. Thus, the results shown in Fig. 10 times 0.424 would result in the efficiency of the CSP system. Since different cycle operating conditions involve different thermal power requirements, the following sections analyze the influence of the limiting pressures and temperatures in the cycle.

3.3. Cycle limiting pressures

Three different solar fields are coupled to s-CO_2 cycles with different low-side pressures. These solar fields are: standard solar tower, multi-heating solar tower with additional heat temperature T_{ah} = 300 °C and optimized concentration ratio, and multi-heating solar tower with additional heat temperature and concentration ratio optimized. Fig. 12 shows cycle, solar field and system efficiencies as a function of low-side pressure. Moreover, the amount of additional thermal power with respect to the total power is also shown for the multi-heating systems.

Cycle efficiency is the same for simple and multi-heating cycles since both types of cycle share the same thermodynamic layout (as explained in Section 2.1). The shape of this curve can be explained with help of Eq. (5). In general terms, when the low-side pressure grows, the compression work (represented by $\dot{W}_c$ in Eq. (5)) decreases and the regeneration irreversibility (represented by $\Delta\dot{H}_{loss}$ in Eq. (5)) increases (González-Portillo et al., 2019). The opposite effect on the cycle efficiency of these two terms results in a maximum cycle efficiency, η_{cycle} = 43.5% at a low-side pressure P_L = 7 MPa.

The reason for the compression work to decrease at high low-side pressures is the change of fluid behavior from gas to liquid-like, and the reason for the regeneration irreversibility to increase is the stronger

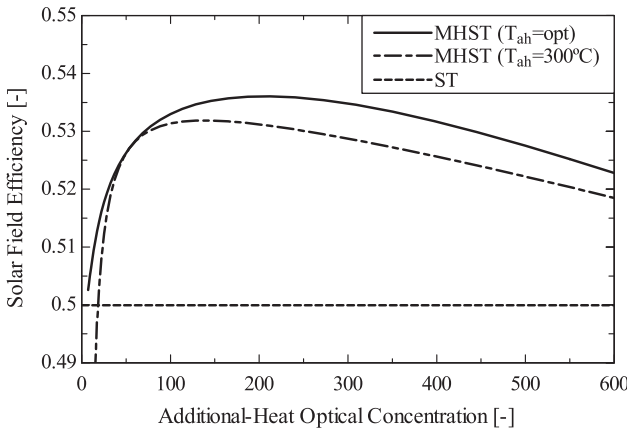

Fig. 10. Solar field efficiency as a function of additional-heat concentration ratio. Solar fields: Solar Tower (ST), Multi-Heating Solar Tower with constant additional heat temperature (MHST - T_{ah} = 300 °C), and Multi-Heating Solar Tower with optimized additional heat temperature (MHST - T_{ah} = opt).

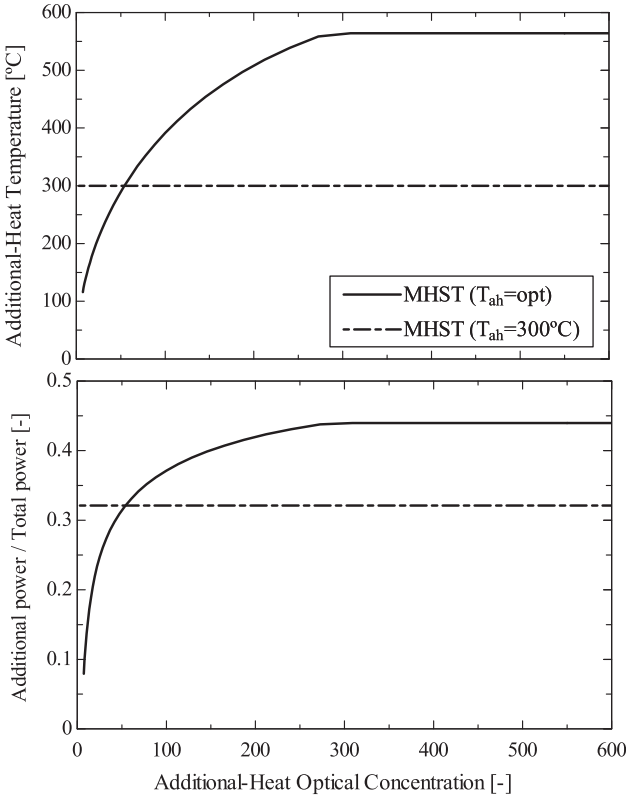

Fig. 11. Additional-heat temperature and portion of additional thermal power as a function of concentration ratio in the additional-heat section of a Multi-Heating Solar Tower with constant additional heat temperature (MHST - T_{ah} = 300 ˚C), and with optimized additional heat temperature (MHST - T_{ah} = opt).

variation of specific heat during the regeneration. In fact, the change of tendency found at 9.5 MPa in the curve of cycle efficiency is due to the strong variation of thermophysical properties across this pressure at the compressor inlet temperature 40 ˚C (González-Portillo et al., 2019). This strong variation of properties involves that, for a temperature of 40 ˚C, the fluid above 9.5 MPa has liquid-like properties and below 9.5 MPa, gas-like properties (González-Portillo et al., 2019). Therefore, when the compressor inlet pressure is below 9.5 MPa, the power consumed by the compressor is high and when the compressor inlet pressure is above 9.5 MPa the power consumed by the compressor is smaller.

The pressure of 9.5 MPa also divides the behavior of the solar field efficiency in the multi-heating systems. When the low-side pressure is low, the term $\Delta\dot{H}_{loss}$ is small and so the cycle can hardly integrate additional heat. The closer the low-side pressure is to 9.5 MPa, the greater the term $\Delta\dot{H}_{loss}$ is due to the increase of variation of thermophysical properties. Thus, the amount of additional thermal power contained in the cycle grows. The greater the amount of additional thermal power, the greater the solar efficiency is. The result is that the solar field efficiency increases with the pressure up to 9.5 MPa, and it barely changes at higher pressures.

The multi-heating solar towers with optimized additional-heat temperature and with additional heat temperature set to T_{ah} = 300 ˚C present similar results. The solar field efficiencies are greater than in the standard system, especially at pressures above 9.5 MPa. The solar field efficiency of the system with the additional-heat temperature optimized is greater than in the system with the additional heat temperature set to T_{ah} = 300 ˚C. However, since the optimized additional-heat temperatures are above 300 ˚C, the system with the additional-heat temperature set to T_{ah} = 300 ˚C has the advantage of softer thermal requirements. A technoeconomic analysis should determine the

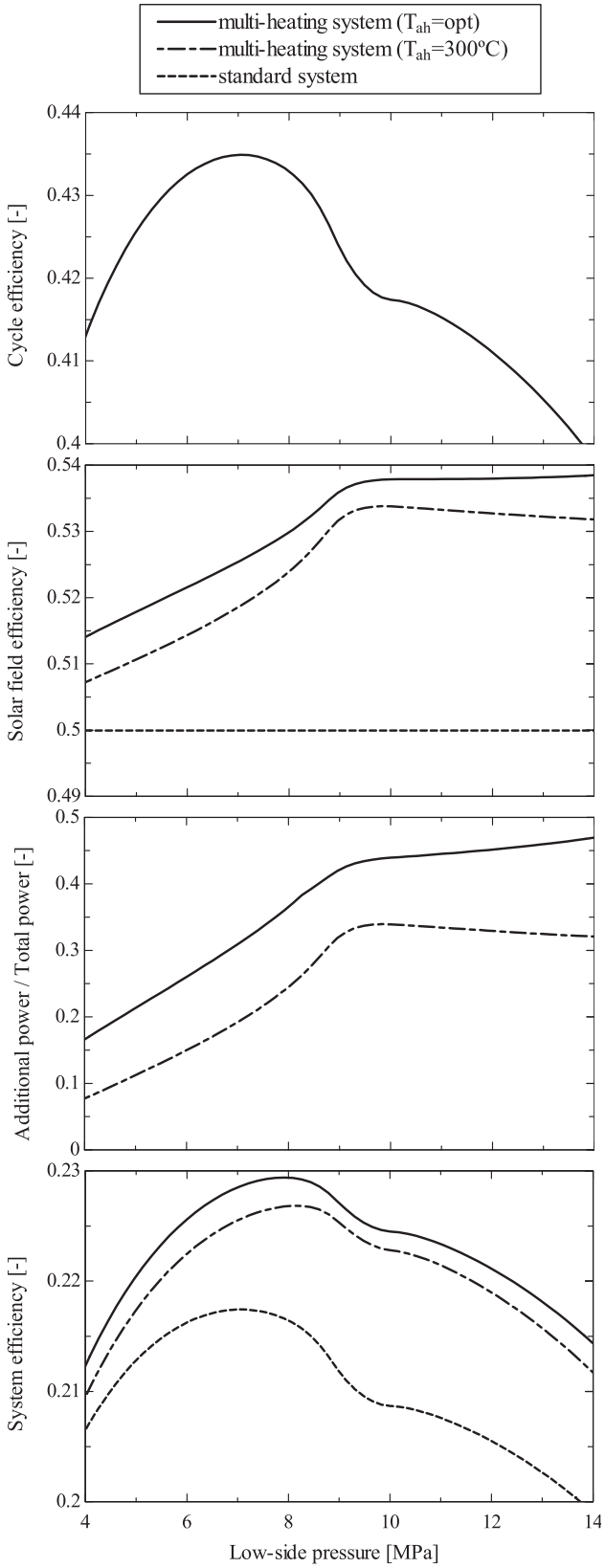

Fig. 12. Cycle efficiency, solar field efficiency, portion of additional thermal power and system efficiency as a function of low-side pressure. Cycle efficiency of simple cycle hides the cycle efficiency of multi-heating cycles since all are the same.

best configuration.

The system efficiency, resulting from coupling cycle and solar efficiencies, shows a shape similar to the cycle efficiency. However, the solar field sets the difference between the systems. The maximum system efficiency is found between 7 MPa and 8 MPa in all the cases. The maximum efficiency of multi-heating is 1.2% greater (a relative difference of 6%) than the maximum efficiency of the standard system. In this case, the additional thermal power of the multi-heating system represents 36% of the total power.

If the purpose were to increase the additional thermal power, the low-side pressure must be increased. If the low-side pressure is increased above 9.5 MPa, e.g., to 10 MPa, the additional thermal power increases up to 44% at the expense of reducing 0.5% the efficiency of the multi-heating system. This means that the multi-heating system would still have an efficiency 0.7% greater than the standard system with maximum efficiency, and almost half of the system would be working at much lower temperature.

The results from Fig. 12 are obtained for a high-side pressure P_H = 25 MPa (defined in Table 1). The influence of the high-side pressure will be analyzed in three systems: standard system with low-side pressure optimized, multi-heating system to maximize the system efficiency (with low-side pressure optimized) and multi-heating system with low-side pressure set to maximize the additional thermal power (low-side pressure P_L = 10 MPa). Fig. 13 shows the influence of the high-side pressure in the efficiency of these systems and in the portion of additional thermal power for the multi-heating systems. Additional heat temperature and concentration ratio are optimized to maximize the solar field efficiency in both multi-heating systems.

The efficiency of the multi-heating system with maximum efficiency (max η) is always higher than the standard system. However, the efficiency of the multi-heating system with maximum additional power (max Q_{ah}) is higher than the standard system only at pressures above P_H = 22.1 MPa. The reason is that, while maximizing the efficiency at low pressures requires small portion of additional power, maximizing the efficiency at high pressures requires big portions of additional power. In fact, both multi-heating systems achieve similar results when the high-side pressure is above 28 MPa.

High-side pressures above P_H = 25 MPa involve higher system efficiency and greater benefit of multi-heating. However, the costs of the system working at these pressures would highly increase. Thus, this study limits the high-side pressure to 25 MPa following the recommendation from the literature (Neises and Turchi, 2019). In this case, the system efficiency of multi-heating is between 0.7% and 1.2% higher than the efficiency of the standard system, and the additional thermal power represents between 36% and 44% of the total.

Low- and high- side pressures have a great influence in multi-heating systems. Figs. 12 and 13 show this influence for a turbine inlet temperature $T_{t,in}$ = 700 °C and a compressor inlet temperature $T_{t,in}$ = 40 °C. Since different temperatures involve different thermal power requirements and efficiencies, the following sections analyze the influence of these temperatures in the system.

3.4. Cycle limiting temperature

Standard and multi-heating systems are analyzed for different turbine inlet temperatures. The goal of the systems is to maximize the efficiency with the variables: low-side pressure, additional-heat temperature and concentration ratio. Fig. 14 shows the efficiency of these systems as a function of turbine inlet temperature. Moreover, the amount of additional thermal power with respect to the total power is also shown for the multi-heating systems.

At low temperatures, the efficiency of standard and multi-heating systems grows due to the increase of cycle efficiency with the temperature (which follows Carnot law). Unlike cycle efficiency, the solar field efficiency decreases with turbine inlet temperature due to the increase of radiation losses with T^4. The opposing effects of cycle and receiver efficiencies result in a system efficiency curve with a maximum. This maximum is achieved at a different turbine inlet temperature depending on the system. This temperature is around 100 °C above the reference turbine inlet temperature from Table 1, 700 °C, which is proposed for the next generation of CSP plants (Mehos et al., 2017). Increasing the turbine inlet temperature beyond 700 °C would involve a higher system efficiency, but also more expensive components. A technoeconomic analysis should evaluate if the increase in efficiency outweighs the increase in cost.

The efficiency of multi-heating systems is greater than the efficiency of standard systems for all the temperatures, but the difference is greater at high temperatures. For example, the increase in efficiency of multi-heating is 1% (relative increase of 5.1%) at turbine inlet temperature $T_{t,in}$ = 500 °C and 1.5% (relative increase of 6.9%) at $T_{t,in}$ = 900 °C. The reason of this difference is the distribution of the heat losses between primary and additional heat. Despite the smaller portion of additional power at high turbine inlet temperatures, substituting part of the heat at high temperature by heat at low temperature highly reduces radiation losses with T^4, and so increases the benefit of multi-heating.

The reason of the smaller portion of additional heat at high turbine inlet temperatures is that, while the total heat increases with the turbine inlet temperature, the additional heat remains almost constant. This is due to the low dependence of the term $\Delta\dot{H}_{loss}$ (which determines the potential of the additional heat) with the turbine inlet temperature since the strong variation of specific heat close to the compressor inlet is the same regardless of the turbine inlet temperature. However, the closer the compressor inlet to the critical temperature, the greater the variation of specific heat (and so the term $\Delta\dot{H}_{loss}$) will be, and so the

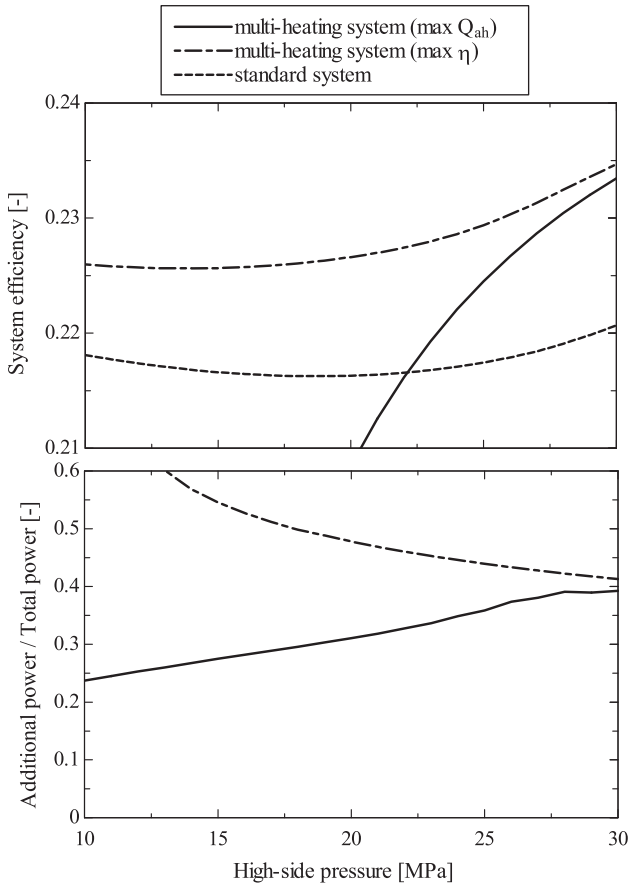

Fig. 13. System efficiency and portion of additional thermal power of three systems: standard system, multi-heating system to maximize the system efficiency (max η) and multi-heating system to maximize the additional thermal power (max Q_{ah}).

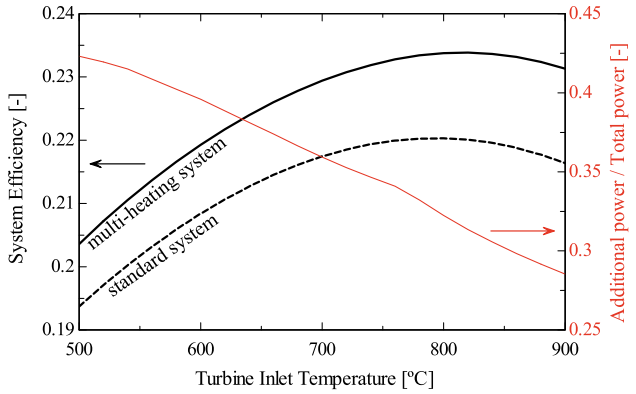

Fig. 14. Efficiency of standard system and multi-heating system as a function of turbine inlet temperature. Portion of additional power in the multi-heating system to the right.

greater the potential of multi-heating. Fig. 15 shows the efficiency of standard and multi-heating systems as a function of compressor inlet temperature. The efficiencies increase at low temperatures, which agrees with Carnot law. But the important feature is that the benefit of multi-heating is greater at lower temperatures.

The reference compressor inlet temperature from Table 1 is $T_{c,in}$ = 40 °C. Reducing this temperature would involve higher system efficiency and greater benefit of multi-heating. However, the compressor inlet temperature is limited by the cold source in terms of heat transfer capacity and temperature. While the use of water could achieve to reduce the compressor inlet temperature to $T_{c,in}$ = 32 °C, the use of air (used in locations with scarce of water) could have more difficulties and typical compressor inlet temperatures are between 40 °C and 55 °C (Ho et al., 2015; Neises and Turchi, 2019). In the reference case, with compressor inlet temperature $T_{c,in}$ = 40 °C, the efficiency of the multi-heating system is 1.2% higher than the standard system, and the additional thermal power is 35.9% of the total. If the compressor inlet temperature could not be below $T_{c,in}$ = 50 °C, then the efficiency of the multi-heating system would still be 1.1% higher than the standard system, and the additional thermal power would be 33.6% of the total.

The objective of this study is to highlight the benefits of multi-heating in CSP systems. However, it is interesting to compare the results obtained for simple and multi-heating cycles with another of the most famous s-CO_2 cycles: the recompression cycle. (Padilla et al., 2015) shows that, at similar conditions to those from Table 1 and compressor inlet temperature $T_{c,in}$ = 32 °C, the cycle efficiency of a recompression cycle is 13.8% higher than the cycle efficiency of a simple cycle. This means that the system efficiency of the standard system with compressor inlet temperature to $T_{c,in}$ = 32 °C shown in Fig. 15, 22.2%, would be increased to 25% if a recompression cycle substituted the simple cycle; and this efficiency would be higher than the system efficiency of a multi-heating system at the same conditions, 23.6%.

CSP systems with recompression cycle will be preferred in terms of efficiency. However, it is hard to say whether they will also be preferred in terms of cost. The higher efficiency of systems with recompression involves a smaller amount of thermal power required for generating a specific electric power, but at the expense of an extra compressor and bigger regenerators. (Neises and Turchi, 2019) show that the cost of CSP systems with simple and recompressor cycle is similar since the lower thermal power required by the recompression cycle is compensated by the extra cost of recompressor and regenerators. For the same reason than recompression cycles, multi-heating cycles will also need bigger regenerators than simple cycles. However, they do not need an extra compressor, and the softer thermal requirements suggest that the cost of the solar field can be greatly reduced. Future research will analyze if the lower thermal requirements of multi-heating cycles can involve a significant decrease in the system cost in comparison to systems with simple and recompression cycle.

4. Conclusions

This work studies the integration of multi-heating s-CO_2 cycles in CSP systems. A new type of solar field, the Multi-Heating Solar Tower, is created for this purpose. The Multi-Heating Solar Tower is divided into two sections: the primary-heat section, with similar conditions than the receiver in a standard Solar Tower, and the additional-heat section, which accommodates the concentration ratio to the low temperatures of this section. The new CSP system with multi-heating is compared to a standard system with simple s-CO_2 cycle and solar tower. The results show that multi-heating achieves a greater efficiency with softer thermal requirements, which involves potential lower costs.

The temperature of the additional heat can be substantially lower than the temperature of the primary heat. In the case of a multi-heating receiver with primary heat temperature T_{ph} = 700 °C and additional heat temperature T_{ph} = 300 °C, the additional thermal power represents a 32% of the total, and the receiver efficiency of the Multi-Heating Solar Tower may be up to 3.1% greater than the receiver efficiency of a standard Solar Tower. If the concentration ratio is decreased in the additional heat section, this difference decreases, but the optical efficiency increases and the thermal requirements get softer. If the concentration ratio is divided by 6 (from $C_{opt,ah}$ = 600 to $C_{opt,ah}$ = 100), the receiver efficiency in the multi-heating solar tower would still be 2.1% greater than the solar tower efficiency, and the optical efficiency would increase from 59.7% to 67%. The result would be a multi-heating solar field (receiver and concentrator) with an efficiency 3.1% higher (a relative increase of 6.2%) than a standard solar field with solar tower.

The system (solar field and cycle) efficiency is analyzed under different operating conditions of the cycle. The low-side pressure is optimized to maximize the system efficiency and to maximize the additional thermal power (which could involve a great benefit in terms of cost). For the reference case with high-side pressure P_H = 25 MPa, the efficiency of the multi-heating system can be up to 1.2% greater (a relative difference of 6%) than the maximum efficiency of the standard system, and the additional thermal power can be up to 44% of the total power. If the high-side pressure lowers then the benefit of multi-heating decreases (in terms of efficiency, of additional thermal power or both)

The efficiency increase of multi-heating systems with respect to standard systems is greater at high turbine inlet temperatures, but the portion of additional heat is smaller at these temperatures. However, low compressor inlet temperatures in multi-heating systems involve both higher increases in efficiency (with respect to standard systems) and larger portions of additional thermal power. Lowering the compressor inlet temperature from 50 °C to 32 °C involves an increase in

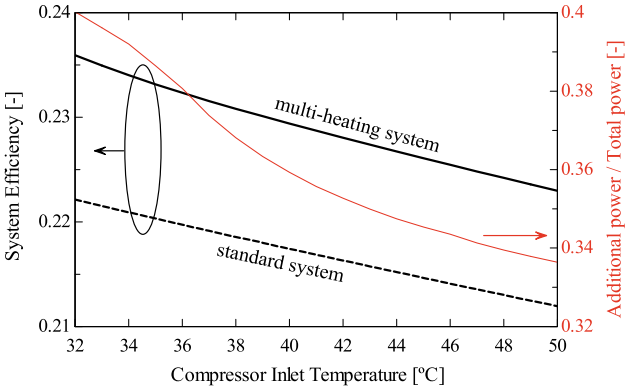

Fig. 15. Efficiency of standard system and multi-heating system as a function of compressor inlet temperature. Portion of additional power in the multi-heating system to the right.

efficiency of multi-heating systems (with respect to standard systems) from 1.1% to 1.4%, and the portion of additional thermal power grows from 33.6% to 40%.

The new CSP system presented in this study uses the basis of thermal coherence to obtain higher efficiencies with lower material requirements. The result (for the reference case) is a system with an efficiency 1.2% (a relative increase of 6%) greater than a standard system and with 44% of the thermal power at low temperature. The smaller surface of heliostats required by a system with higher efficiency and the softer requirements in temperature and concentration ratio give the multi-heating system a great potential to reduce the cost of electricity. This cost reduction will have to overcome the greater cost of bigger regenerators that will probably be associated to multi-heating cycles. In order to confirm the potential of multi-heating, future work will have to focus on the techno-economic analysis of this system and compare the resulting cost of electricity with the rest of options proposed for the next generation of CSP plants.

Declaration of Competing Interest

The authors declare that they have no known competing financial interests or personal relationships that could have appeared to influence the work reported in this paper.

Acknowledgments

The authors thank to “Comunidad de Madrid” and European Structural Funds for their financial support to ACES2030-CMproject (S2018/EMT-4319). Technical discussions with other members of the research group “Grupo de Investigaciones Termoenergéticas” from the Universidad Politécnica de Madrid were essential for this work.

Appendix

Annual simulations are carried out in System Advisor Model (SAM) version 2018.11.11 to obtain the receiver efficiencies shown in Fig. 5. The performance model used is “CSP power tower molten salt”. All parameters except HTF temperatures are default values. Two different cases are simulated:

- Case 1: HTF hot temperature 500 ˚C and HTF cold temperature 250 ˚C
- Case 2: HTF hot temperature 800 ˚C and HTF cold temperature 550 ˚C

The values shown in Fig. 5 belong to the hourly receiver efficiency along a year for both cases. Since the solar flux hitting the receiver varies hourly, it is possible to obtain the receiver efficiency for several different solar heat fluxes. The receiver efficiency is calculated by using hourly outputs as follows:

$$\eta_{rec} = 1 - \frac{Rec.\ \ convection\&emission\ losses + Rec.\ \ header/tower\ piping\ losses}{Rec.\ \ incident\ thermal\ power}$$

And the solar heat flux:

$$Radiation\ flux\ hitting\ receiver = \frac{Rec.\ \ incident\ thermal\ power}{Rec.\ \ area}$$

The values from hours where the plant starts to work are discarded since they include startup thermal energy losses.

References

Ahn, Y., Bae, S.J., Kim, M., Cho, S.K., Baik, S., Lee, J.I., Cha, J.E., 2014. Cycle layout studies of S-CO2 cycle for the next generation nuclear system application. Transactions of the Korean Nuclear Society Autumn Meeting Pyeongchang 2–5.

Albrecht, K.J., Bauer, M.L., Ho, C.K., 2019. Parametric Analysis of Particle CSP System Performance and Cost to Intrinsec Particle Properties and Operating Conditions, in: 13th International Conference on Energy and Sustainability.

Binotti, M., Astolfi, M., Campanari, S., Manzolini, G., Silva, P., 2017. Preliminary assessment of sCO2 cycles for power generation in CSP solar tower plants. Appl. Energy 204, 1007–1017. https://doi.org/10.1016/J.APENERGY.2017.05.121.

Bryant, J.C., Saari, H., Zanganeh, K., 2011. An analysis and comparison of the simple and recompression supercritical CO2 cycles. Supercritical CO2 Power Cycle Symposium.

Crespi, F., Gavagnin, G., Sánchez, D., Martínez, G.S., 2017. Supercritical carbon dioxide cycles for power generation: A review. Appl. Energy 195, 152–183. https://doi.org/10.1016/J.APENERGY.2017.02.048.

Dostal, V., 2004. A supercritical carbon dioxide cycle for next generation nuclear reactors. PhD Thesis. PhD Thesis. Massachusetts Institute of Technology.

Dyreby, J., 2014. Modeling the Supercritical Carbon Dioxide Brayton Cycle with Recompression. PhD Thesis. The University of Wisconsin, Madison.

EnergyPlus, 2018. Weather Data Base [WWW Document]. URL https://energyplus.net/weather (accessed 5.8.18).

Enríquez, L.C., Muñoz-Antón, J., Peñalosa, J.M.M.V., 2017. Thermodynamic optimization of supercritical CO2 brayton power cycles coupled to line-focusing solar fields. J. Sol. Energy Eng., Trans. ASME 139, 1–8. https://doi.org/10.1115/1.4037381.

Forristall, R., 2003. Heat transfer analysis and modeling of a parabolic trough solar receiver implemented in engineering equation solver. NREL/TP-550-34169.

González-Portillo, L.F., Muñoz-Antón, J., Martínez-Val, J.M., 2020. Thermodynamic analysis of multi-heating cycles working around the critical point. Appl. Therm. Eng. 174, 115292. https://doi.org/10.1016/j.applthermaleng.2020.115292.

González-Portillo, L.F., Muñoz-Antón, J., Martínez-Val, J.M., 2019. Thermodynamic mapping of power cycles working around the critical point. Energy Convers. Manage. 192, 359–373. https://doi.org/10.1016/j.enconman.2019.04.022.

González-Portillo, L.F., Muñoz-Antón, J., Martínez-Val, J.M., 2017. An analytical optimization of thermal energy storage for electricity cost reduction in solar thermal electric plants. Appl. Energy 185, 531–546. https://doi.org/10.1016/j.apenergy.2016.10.134.

Ho, C.K., 2017. Advances in central receivers for concentrating solar applications. Sol. Energy 152, 38–56. https://doi.org/10.1016/J.SOLENER.2017.03.048.

Ho, C.K., Carlson, M., Garg, P., Kumar, P., 2016. Technoeconomic analysis of alternative solarized s-CO 2 brayton cycle configurations. J. Sol. Energy Eng. 138, 051008. https://doi.org/10.1115/1.4033573.

Ho, C.K., Carlson, M., Garg, P., Kumar, P., 2015. Cost and performance tradeoffs of alternative solar-driven S-CO2 brayton cycle configurations. In: Proceedings of the ASME 2015 Power and Energy Conversion Conference 1–10, https://doi.org/10.1115/ES2015-49467.

Ho, C.K., Iverson, B.D., 2014. Review of high-temperature central receiver designs for concentrating solar power. Renew. Sustain. Energy Rev. 29, 835–846. https://doi.org/10.1016/j.rser.2013.08.099.

Kim, Y.M., Kim, C.G., Favrat, D., 2012. Transcritical or supercritical CO2 cycles using both low- and high-temperature heat sources. Energy 43, 402–415. https://doi.org/10.1016/j.energy.2012.03.076.

Klein, S., 1992. Engineering Equation Solver (EES).

Linares, J.I., Herranz, L.E., Fernández, I., Cantizano, A., Moratilla, B.Y., 2015. Supercritical CO2 Brayton power cycles for DEMO fusion reactor based on Helium Cooled Lithium Lead blanket. Appl. Therm. Eng. 76, 123–133. https://doi.org/10.1016/j.applthermaleng.2014.10.093.

Mehos, M., Turchi, C., Vidal, J., Wagner, M., Ma, Z., Ho, C., Kolb, W., Andraka, C., Kruizenga, A., 2017. Concentrating Solar Power Gen3 Demonstration Roadmap. NREL/TP-5500-67464.

Montes, M.J., Abánades, A., Martínez-Val, J.M., Valdés, M., 2009. Solar multiple optimization for a solar-only thermal power plant, using oil as heat transfer fluid in the parabolic trough collectors. Sol. Energy 83, 2165–2176. https://doi.org/10.1016/j.solener.2009.08.010.

Muñoz-Anton, J., Biencinto, M., Zarza, E., Díez, L.E., 2014. Theoretical basis and experimental facility for parabolic trough collectors at high temperature using gas as heat transfer fluid. Appl. Energy 135, 373–381. https://doi.org/10.1016/j.apenergy.2014.08.099.

Muñoz-Antón, J., Rubbia, C., Rovira, A., Martínez-Val, J.M., 2015. Performance study of

solar power plants with CO2 as working fluid. A promising design window. Energy Convers. Manage. 92, 36–46. https://doi.org/10.1016/j.enconman.2014.12.030.
Muñoz, J., Abánades, A., Martínez-Val, J.M., 2009. A conceptual design of solar boiler. Sol. Energy 83, 1713–1722. https://doi.org/10.1016/j.solener.2009.06.009.
Muñoz, J., Martinez-Val, J.M., Ramos, A., 2011. Thermal regimes in solar-thermal linear collectors. Sol. Energy 85, 857–870. https://doi.org/10.1016/j.solener.2011.02.004.
Neises, T., Turchi, C., 2019. Supercritical carbon dioxide power cycle design and configuration optimization to minimize levelized cost of energy of molten salt power towers operating at 650 °C. Sol. Energy 181, 27–36. https://doi.org/10.1016/J.SOLENER.2019.01.078.
Neises, T., Turchi, C., 2014. A comparison of supercritical carbon dioxide power cycle configurations with an emphasis on CSP applications. Energy Procedia 49, 1187–1196. https://doi.org/10.1016/j.egypro.2014.03.128.
Neises, T.W., Wagner, M.J., Gray, A.K., 2014. Structural design considerations for tubular power tower receivers operating at 650°C. NREL/CP-5500-61848 1–7.
NREL, 2018. SAM (System Advisor Model) version 2018.11.11.
Padilla, R.V., Soo Too, Y.C., Benito, R., Stein, W., 2015. Exergetic analysis of supercritical CO2 Brayton cycles integrated with solar central receivers. Appl. Energy 148, 348–365. https://doi.org/10.1016/j.apenergy.2015.03.090.
Padilla, R.V., Too, Y.C.S., Benito, R., McNaughton, R., Stein, W., 2016. Thermodynamic feasibility of alternative supercritical CO2 Brayton cycles integrated with an ejector. Appl. Energy 169, 49–62. https://doi.org/10.1016/j.apenergy.2016.02.029.
Rovira, A., Rubbia, C., Valdés, M., Martínez-Val, J.M., 2014. Thermodynamic cycles optimised for medium enthalpy units of concentrating solar power. Energy 67, 176–185. https://doi.org/10.1016/j.energy.2014.02.029.
Swinbank, W.C., 1963. Long-wave radiation from clear skies. Q. J. R. Meteorolog. Soc. 89, 339–348. https://doi.org/10.1002/qj.49708938105.
Syblik, J., Vesely, L., Entler, S., Stepanek, J., Dostal, V., 2019. Analysis of supercritical CO2 Brayton power cycles in nuclear and fusion energy. Fusion Eng. Des. 146, 1520–1523. https://doi.org/10.1016/j.fusengdes.2019.02.119.
Wagner, M.J., Wendelin, T., 2018. SolarPILOT: A power tower solar field layout and characterization tool. Sol. Energy 171, 185–196. https://doi.org/10.1016/J.SOLENER.2018.06.063.
Wang, G., Niu, S., Yu, S., Lin, J., Chen, Z., Hu, P., 2020. Parametric study on integrated thermal and mechanical performance of molten salt receiver for solar tower power plant. Int. J. Thermophys. 41, 1–17. https://doi.org/10.1007/s10765-020-2603-4.
Wang, K., He, Y.-L., Zhu, H.-H., 2017. Integration between supercritical CO2 Brayton cycles and molten salt solar power towers: A review and a comprehensive comparison of different cycle layouts. Appl. Energy 195, 819–836. https://doi.org/10.1016/J.APENERGY.2017.03.099.